Magnetic structure of $HoBe_{13}$ in an applied magnetic field

P. Dervenagas, P. Burlet, M. Bonnet, and F. Bourdarot
Commissariat à l'Energie Atomique, Département de Recherche Fondamentale sur la Matière Condensée, SPSMS/MDN, 38054 Grenoble Cedex 9, France

A. Hiess
Institut Laue-Langevin, 156 X, 38042 Grenoble, France

S. L. Bud'ko and P. C. Canfield
Ames Laboratory and Department of Physics and Astronomy, Iowa State University, Ames, Iowa 50011

G. H. Lander
European Commission, JRC, Institute for Transuranium Elements, Postfach 2340, D-76125 Karlsruhe, Germany

J. S. Kim and G. R. Stewart*
Department of Physics, University of Florida, Gainesville, Florida 32611-8440
(Received 20 July 1998; revised manuscript received 5 August 1999)

The magnetic structure of $HoBe_{13}$ and its evolution under an applied magnetic field have been examined using neutron diffraction and bulk magnetization measurements on a single crystal. In the absence of an external field this cubic compound orders at $T_N = 5.7(1)$ K into a regular helical magnetic structure with propagation vector $\mathbf{k} = [0\,0\,\frac{1}{3}]$. Third-order harmonics appear at 4.4(1) K and are attributed to a deformation of the helical structure below this temperature. When a magnetic field is applied along a [001] axis two magnetic transitions occur. First the magnetic domain with propagation vector parallel to the field is favored and, with the addition of the induced ferromagnetic component, by about 4 kG we have a single-domain conical structure. The surprising observation was that at higher fields (15 kG at 1.4 K) the other two domains reappear and become the preferred ones. This reentrant behavior is due to the change of the magnetic structure to a canted arrangement, involving a ferromagnetic component along the applied field and a transverse collinear antiferromagnetic component. When the magnetic field is applied along a [110] axis only one transition is observed from the helical to the conical structure. The magnetic phase diagram of $HoBe_{13}$ has been constructed.

I. INTRODUCTION

The family of beryllides MBe_{13}, where M can be an alkali-earth element, a rare earth including Sc and Y, an actinide, as well as some of the $4d$ and $5d$ transition elements, has been the subject of interest for many years.[1] These compounds crystallize in the cubic $NaZn_{13}$-type structure (space group $Fm\bar{3}c$) and the separation between M atoms is always greater than 5 Å. As a result, when M is a rare earth, the direct exchange interaction is very small and the dominant role is played by indirect exchange interactions of the Ruderman-Kittel-Kasuya-Yosida type mediated by the conduction electrons which are coming primarily from the beryllium atoms. The rare-earth compounds RBe_{13} with R = Gd, Tb, Dy, Ho, and Er order antiferromagnetically with transition temperatures T_N that obey de Gennes' law, as revealed by magnetic measurements.[1,2] Vigneron *et al.* investigated the magnetic structures of the above-mentioned compounds using neutron-diffraction techniques on powder samples.[3–6] It was found that the magnetic structures of $ErBe_{13}$ and $DyBe_{13}$ are helical ones with propagation vector $[0\,0\,\frac{1}{3}]$. $GdBe_{13}$ exhibits a similar structure with a propagation vector [0 0 0.285] which apparently is independent of temperature. On the other hand, $TbBe_{13}$ and $HoBe_{13}$ order also into a helical structure, which is incommensurate at T_N, and gradually shifts into a commensurate one at a lower temperature T_{N_1}. The variation of the ordering wave vector with temperature for these two compounds can be described by $\frac{1}{3}\mathbf{c}^*[1-\epsilon(T)]$. A mean-field approximation model which includes isotropic exchange interactions between localized $4f$ moments and magnetocrystalline anisotropy has been proposed[6,7] in order to account for the magnetic structures of the RBe_{13} family.

For $HoBe_{13}$ which is our main interest here, the wave vector was reported[6] to start at the incommensurate value [0 0 0.328] at $T_N = 6$ K and become commensurate at $T_{N_1} = 4.5$ K. Below this temperature third-order harmonics are observed corresponding to a deformation of the helical structure.

Recently the magnetic structure of the isostructural actinide compound $NpBe_{13}$ has been determined.[8] It was found that the magnetic wave vector has also the value $[0\ 0\ \frac{1}{3}]$, although the arrangement of the magnetic moments is different from that found in the RBe_{13} compounds. We should note that UBe_{13} is the only uranium-based heavy fermion superconductor in which no magnetic correlations have been reported despite efforts with muons[9] and neutrons.[10,11]

Single crystals of $HoBe_{13}$ have been produced at the Uni-

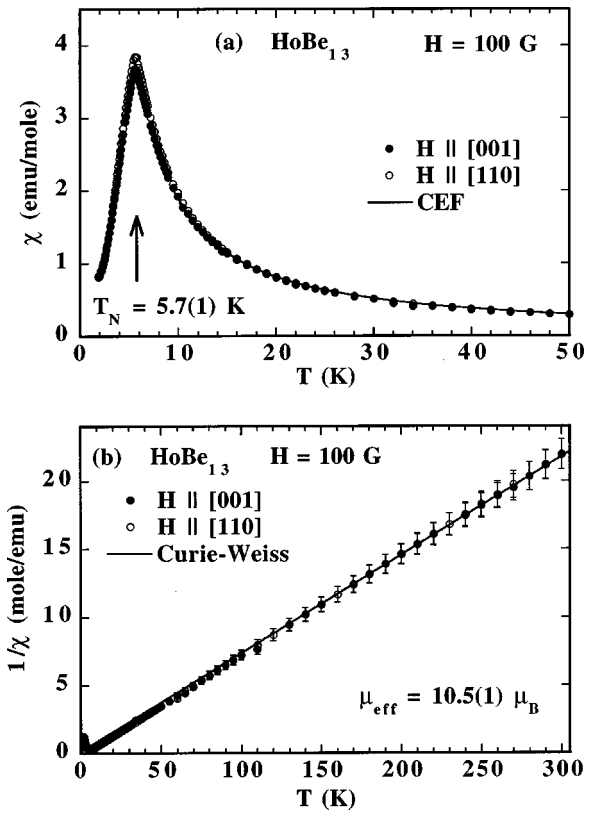

FIG. 1. (a) Temperature dependence of the magnetic susceptibility of $HoBe_{13}$ in a 100 G applied field. For clarity we show only the data up to 50 K. The solid line is the calculation using the CEF model described in the text. The data were fitted in the paramagnetic region, down to 10 K. (b) The inverse of the susceptibility. The fit to the Curie-Weiss law was performed on the data above 150 K.

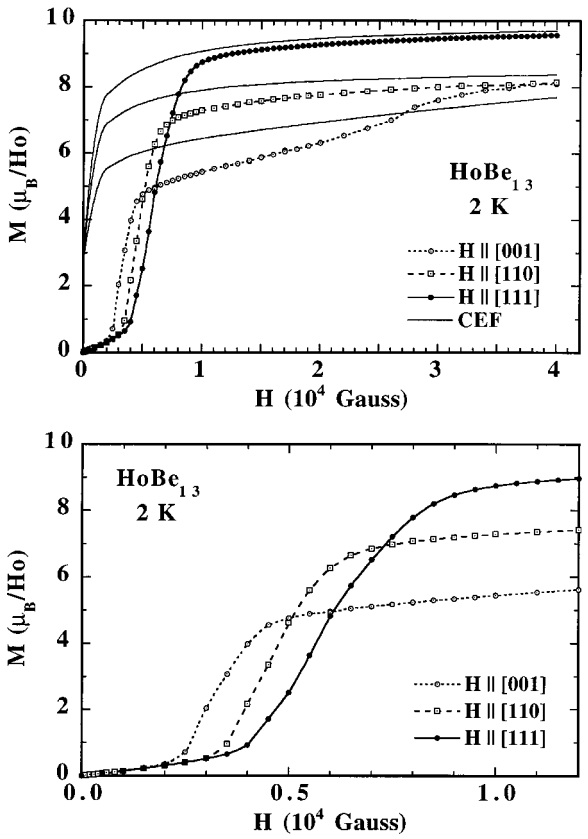

FIG. 2. In the upper panel we present the magnetization curves of $HoBe_{13}$ versus applied magnetic field along the high-symmetry directions at 2 K. The CEF model calculations (solid lines) account well for the anisotropy at high magnetic fields. In the lower panel the low-field data are presented in more detail. We observe that the presence of the antiferromagnetic structure leads to a complicated metamagnetic behavior.

versity of Florida using an Al flux growth procedure in an outgassed BeO crucible with lid sealed in Ta. This allowed us to reexamine the magnetic structure of this material, and to study what happens when an external magnetic field is applied.

II. MAGNETIZATION

Magnetic susceptibility and magnetization measurements were performed on a 8.7 mg single crystal of $HoBe_{13}$ using a Quantum Design superconducting quantum interference device magnetometer. Measurements were performed in the temperature range $1.9 \leqslant T \leqslant 300$ K, with the magnetic field applied along the [001], [110], and [111] high-symmetry directions. The low-field magnetic susceptibility is almost isotropic, as we can see in Fig. 1(a) where we present measurements in an applied field of 100 G for two orientations. The antiferromagnetic transition temperature is found to be $T_N = 5.7(1)$ K in good agreement with the previously published results. The inverse of the susceptibility $1/\chi(T)$ versus T is plotted in Fig. 1(b). It is evident that the data follow a Curie-Weiss behavior,

$$\chi = \frac{C}{T-\theta} = \frac{N\mu_{\text{eff}}^2}{3k_B(T-\theta)}, \tag{1}$$

where C is the Curie constant, θ is the Weiss temperature, N is the number of Ho^{+3} ions, and μ_{eff} is the effective magnetic moment per ion. From the slope of $1/\chi(T)$ for the high-temperature region $150 \leqslant T \leqslant 300$ K, μ_{eff} for the Ho^{+3} ion is found to be $10.5(1)\mu_B$, in good agreement with the theoretical value of $10.63\mu_B$ predicted from the Hund's rule ground state of the free Ho^{+3} ion. The Weiss temperature is found to be $\theta = -2.1 \pm 1.0$ K.

Isothermal magnetization curves as a function of applied field were also determined for a number of temperatures between 1.9 and 6 K. In Fig. 2 we plot the curves corresponding to the three field directions at 2 K (below T_N). At 40 kG the magnetization is about $8.1\mu_B$ per Ho^{+3} ion along the [001] and [110] axis, while it reaches $9.6\mu_B$ per Ho^{+3} ion along the [111] axis. We can, therefore, say that the [111] axis is the spontaneous easy axis of magnetization. At low fields, the exchange interactions associated with the magnetic order lead to a quite complex metamagnetic behavior, as we can see clearly in the lower panel of Fig. 2. We observe two distinct magnetic transitions when the field is applied along the [001] axis, but only one with a field applied along the [110] or [111] directions. The results of the magnetization measurements will be discussed in the light of the neutron-diffraction study that follows.

A crystal electric field (CEF) model has been used to fit the temperature dependence of the low-field magnetic sus-

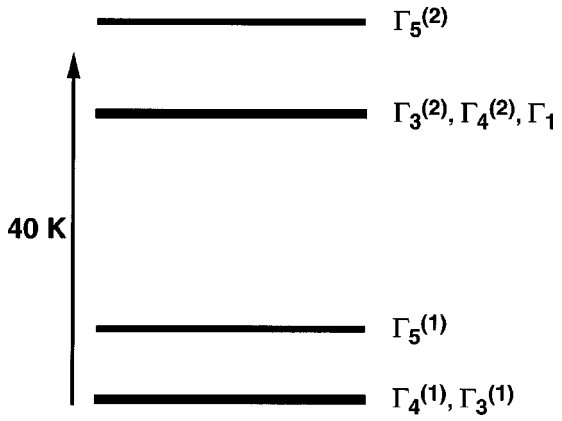

FIG. 3. Paramagnetic CEF energy-level scheme of $HoBe_{13}$. The ground state is a mixture of a nonmagnetic $\Gamma_3^{(1)}$ and a magnetic $\Gamma_4^{(1)}$ level. The three levels around 32 K are also quasidegenerate.

ceptibility in the paramagnetic state (down to 10 K). We have also included in the fit the high-field magnetization data at 2 K, in order to account for the observed anisotropy. At high fields the antiferromagnetic structure is broken, and we are justified in doing so. The Hamiltonian describing the magnetic properties of a $4f$ shell in the paramagnetic phase and for cubic symmetry is written as[12]

$$\mathcal{H}=\mathcal{H}_{\mathrm{CEF}}+\mathcal{H}_Z+\mathcal{H}_B. \tag{2}$$

$\mathcal{H}_{\mathrm{CEF}}$ is the CEF term which is written using the operator equivalent method as

$$\mathcal{H}_{\mathrm{CEF}}=\beta_J V_4(O_4^0+5O_4^4)+\gamma_J V_6(O_6^0-21O_6^4), \tag{3}$$

where β_J, γ_J are Stevens coefficients, O_l^m is the Stevens equivalent operators, and V_l^m is the CEF parameters:[13]

$$\mathcal{H}_Z=-g_J\mu_B\mathbf{H}\cdot\mathbf{J} \tag{4}$$

represents the Zeeman coupling between the $4f$ magnetic moment and the internal magnetic field (external field corrected for demagnetization effects). Finally,

$$\mathcal{H}_B=-g_J\mu_B\mathbf{H}_{\mathrm{ex}}\cdot\mathbf{J} \tag{5}$$

is the Heisenberg-type isotropic bilinear interaction Hamiltonian written in the mean-field approximation, with the exchange field $\mathbf{H}_{\mathrm{ex}}$ given by

$$\mathbf{H}_{\mathrm{ex}}=n\mathbf{M}=ng_J\mu_B\langle\mathbf{J}\rangle, \tag{6}$$

where n is the isotropic bilinear exchange parameter. The anisotropic bilinear couplings, as well as higher-order couplings are neglected here.

The CEF model accounts very well for the temperature dependence of the susceptibility, as is evident from Fig. 1(a). We find $V_4=-10.77$ K, $V_6=3.06$ K, and $n=1.33$ kG/μ_B for the fitted parameters. In the upper panel of Fig. 2 we plot the calculated magnetization curves using our model. We see that at high fields the agreement is reasonable, so the anisotropy may be attributed to CEF effects. At low fields, where the antiferromagnetic structure is present, the CEF model alone cannot provide good agreement with the observed magnetization curves. The calculated paramagnetic CEF level scheme of $HoBe_{13}$ is presented in Fig. 3. We find that the degeneracy of the $J=8$ multiplet is not completely raised, so that the ground state is a mixture of a nonmagnetic $\Gamma_3^{(1)}$ and a magnetic $\Gamma_4^{(1)}$ level. Efforts to investigate the CEF level scheme of $HoBe_{13}$ by means of neutron inelastic scattering measurements on powder samples where unsuccesful.[14] They were successful, however, in the case of $ErBe_{13}$ where an overall CEF splitting of 38 K, comparable with our calculation here was measured.[15]

III. NEUTRON DIFFRACTION

Neutron-diffraction measurements on a 20 mg single crystal of $HoBe_{13}$ were performed using the D15 diffractometer at the ILL reactor. The crystal was from the same batch as the one used for the magnetization measurements and it was placed in a cryomagnet which could provide a vertical magnetic field of up to 50 kG and temperatures down to 1.4 K. The diffractometer was operated in the normal beam mode with a wavelength of 1.174 Å and its detector, in the presence of the magnet, could move from $-7°$ below to 17° above the horizontal plane.

A. Crystal structure

$HoBe_{13}$ crystallizes in the face-centered-cubic $NaZn_{13}$ structure (space group $Fm\bar{3}c$), which has eight formula units in the cubic unit cell. The Ho atoms occupy eight equivalent positions at $(\frac{1}{4}\ \frac{1}{4}\ \frac{1}{4})$, $(\frac{3}{4}\ \frac{3}{4}\ \frac{3}{4})$, while Be has two inequivalent positions, 8 Be_I at $(0\ 0\ 0)$, $(\frac{1}{2}\ \frac{1}{2}\ \frac{1}{2})$, and 96 Be_{II} at $(0\ \ y\ \ z)$. Each Ho atom is surrounded by a polyhedron of 24 Be_{II} atoms and by a cube of 8 Be_I atoms. What is important for the study of the magnetic structure that follows, is to notice that the Ho atoms form a simple cubic lattice with lattice parameter $a/2$, and that there are two layers of Ho atoms in the cubic cell of $HoBe_{13}$. In our experiment, the lattice parameter was determined to be $a=10.205$ Å at 8 K and changes very little with temperature.

In order to verify the crystal structure of our sample, the integrated intensities of 60 nuclear Bragg reflections were measured in the paramagnetic state at 8 K. Intensities were measured by rotating the crystal around the vertical axis through the reflections. The data were corrected for absorption, although these corrections are small. A least-squares refinement of the intensities gave structural parameters of $y=0.1147(4)$ and $z=0.1787(3)$ in agreement with previously determined values.[6] The agreement between observed and calculated intensities, given by the factor $R=\Sigma\left|\sqrt{(I/L)_{\mathrm{obs}}}-\sqrt{(I/L)_{\mathrm{cal}}}\right|/\Sigma\sqrt{(I/L)_{\mathrm{obs}}}$, was found to be 2.5%. Here L is the geometrical Lorentz factor. We also obtained the scale factor between the observed and calculated intensities, the temperature parameters for the Debye-Waller factor, and the extinction parameters.

The extinction corrections are small, being less than 5% for most reflections except for the strongest ones. The same group of nuclear integrated intensities was measured at 5.2 K (just below T_N) and at 1.4 K and no changes were observed.

B. Zero-field magnetic structure

When the sample is cooled below the transition temperature $T_N=5.7(1)$ K, magnetic peaks appear at positions in

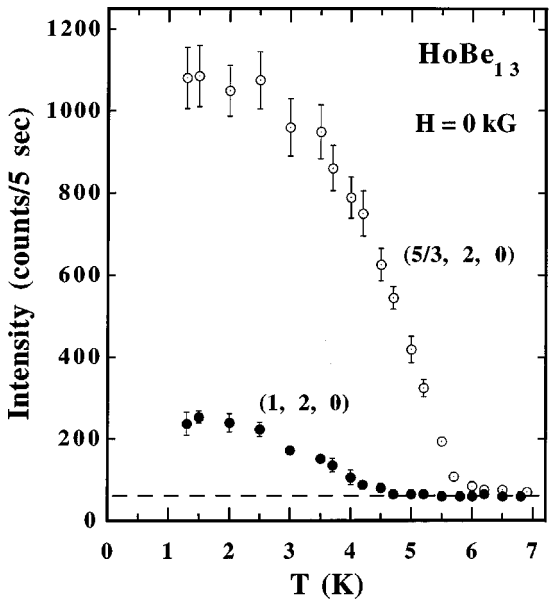

FIG. 4. Temperature dependence of the intensities of the $(\frac{5}{3}\ 2\ 0)$ magnetic peak and the corresponding third-order harmonic (1 2 0) at zero field. The values are peak intensities from scans along the [100] direction.

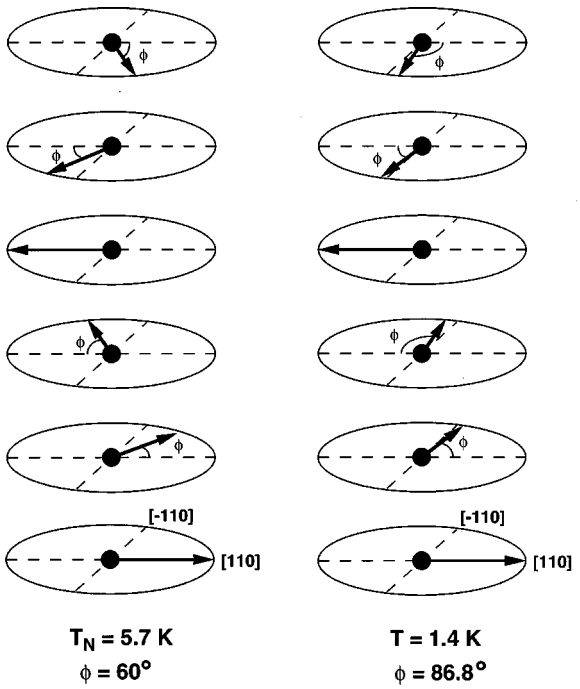

FIG. 5. Zero-field magnetic structure of $HoBe_{13}$ for a propagation vector $[0\ 0\ \frac{1}{3}]$ along the z direction. Each atom represents a layer of Ho atoms perpendicular to the z axis. At the transition temperature T_N we have a regular helix which becomes deformed below 4.4(1) K. As explained in the text, we have chosen the initial phase so that the moments are close to the [110] directions. The deformation of the helix at low temperatures is necessary in order to explain the appearance of third-order harmonics. The value of ϕ at 1.4 K is very close to 90° so that the moments are effectively along the [110] axes.

reciprocal space of the type $\mathbf{Q}=\mathbf{G}\pm\mathbf{k}$, where $\mathbf{G}$ is the reciprocal-lattice vector of any allowed nuclear Bragg peak, and $\mathbf{k}$ is one of the equivalent magnetic ordering wave vectors $[\frac{1}{3}\ 0\ 0]$,$[0\ \frac{1}{3}\ 0]$, and $[0\ 0\ \frac{1}{3}]$. The allowed nuclear reflections $(h\ k\ l)$ which contain contributions from the Ho atoms have all indices even. On further cooling, additional peaks appear below 4.4(1) K at positions $\mathbf{Q}=\mathbf{G}\pm 3\mathbf{k}$, as shown in Fig. 4 which presents the intensities of the $(\frac{5}{3}\ 2\ 0)$ magnetic peak and the corresponding third-order harmonic (1 2 0) as a function of temperature. As we mentioned in the Introduction, in the previous examination of $HoBe_{13}$ using a powder sample, it was found that the magnetic wave vector is initially incommensurate. At 4.9 K the wave vector was found to be [0 0 0.328].[6] In our experiment we have not observed any such departure from the commensurate value $[0\ 0\ \frac{1}{3}]$. However, our best resolution in the present experiment was about 0.005 rlu, so one has to resort to higher resolution measurements to be certain.

We use the helical model proposed by Vigneron *et al.*[6] to analyze the intensities of the magnetic peaks. In this model, the Ho atoms in each layer perpendicular to the magnetic wave vector are ferromagnetically aligned and the direction of the moments rotates as we move from one layer to the next, so that the magnetic unit cell is tripled in the direction of the propagation vector, as shown in Fig. 5. Using this model and the standard formalism of magnetic diffraction[16] we obtain the following expressions for the integrated intensities of the first and third-order harmonics:

$$I_{\mathbf{k}}=KL(\mathbf{Q})p^2f^2(\mathbf{Q})\frac{1}{54}[(1+\cos\phi)^2 + 3\sin^2\phi]\left\{1+\frac{Q_{||}^2}{\mathbf{Q}^2}\right\}m^2, \quad (7)$$

$$I_{3\mathbf{k}}=KL(\mathbf{Q})p^2f^2(\mathbf{Q})\frac{1}{54}(1-2\cos\phi)^2\left\{1+\frac{Q_{||}^2}{\mathbf{Q}^2}\right\}m^2, \quad (8)$$

where K is the scale factor determined from the analysis of the nuclear intensities and $L(\mathbf{Q})=1/\sin 2\theta\cos\mu$ is the geometrical Lorentz factor (2θ is the projection of the scattering angle in the horizontal plane and μ is the angle out of this plane). $p=0.2696\times10^{-12}$ cm, and $f(\mathbf{Q})$ is the magnetic form factor of the Ho^{3+} ion. $Q_{||}$ is the component of the scattering vector $\mathbf{Q}$ parallel to the direction of the propagation vector. For example, for $\mathbf{k}=[0\ \frac{1}{3}\ 0]$, $Q_{||}=Q_y$. Finally, ϕ is the angle in Fig. 5 and m is the value of the ordered magnetic moments, which are the parameters to be determined by the measurements. In the above expressions we have taken into account that the crystal is divided into domains with propagation vectors along the x, y, and z directions, and we have assumed equipartition between domains. For each domain we have taken the average between equivalent configurations. Absorption and extinction corrections are of the order of 1% for the more intense magnetic peaks and we can ignore them. The Debye-Waller factor for the Ho atoms at the temperatures of interest is also negligible (corrections less than 0.3%) and has been omitted in the formulas. We also note that the intensities do not depend on the initial phase. In Fig. 5 we have plotted the moments as being close to the [110] axes, a choice consistent with both the

magnetization measurements (Fig. 2) and the diffraction experiments under magnetic field which we discuss later in the paper.

From Eq. (8) we see that when $\phi = 60°$, which is when the helical magnetic structure is regular, the intensity of the third-order harmonics is zero. In order to account for their existence at low temperatures we have to let ϕ take different values, creating a deformed helical structure. The integrated intensities of magnetic peaks were collected at 5.2 K where only first harmonics exist, and at 1.4 K the lowest temperature that we could reach.

To analyze the magnetic intensities at 5.2 K we use Eq. (7) with $\phi = 60°$. By adjusting the value of the ordered moment so that the calculated intensities best agree with the measured ones, we find $m = 4.0(2)\mu_B$ per Ho atom. The agreement between the observed and the calculated intensities, given now by the factor $R = \Sigma|(I/L)_{\rm obs} - (I/L)_{\rm cal}|/\Sigma(I/L)_{\rm obs}$, is 6.5%. For convenience, in this paper we work with integrated intensities normalized by the Lorentz factor L.

At 1.4 K we have two parameters ϕ and m. Again we calculate the values of these parameters that provide the best agreement between observed and calculated intensities. We find that $\phi = 86.8(1.0)°$ and $m = 7.7(3)\mu_B$ (R factor of 6.0%). These values are in agreement with the previous results.[6] The value of ϕ is so close to 90° that effectively all the moments are along the [110] directions.

We should note that the zero-field magnetic structure can be described also as a transverse sinusoidal modulation of the moments, which would become squared at low temperatures to account for the third-order harmonics. This model can fit the magnetic intensities equally well but it is incompatible with the evolution of the magnetic structure under an applied magnetic field which we discuss below.

C. Magnetic structure in an applied magnetic field

As is evident from the magnetization measurements (Fig. 2) it is interesting to examine the magnetic structure under a magnetic field applied along the [001] and [110] axes. For a field along [001] we found that, as the field increases, initially the intensities of the magnetic reflections with propagation vectors parallel to the field increase while the others decrease rapidly. This means that the domains propagating along the **c** axis, which have their magnetic moments in planes normal to the magnetic field, are energetically favored as expected. By about 4 kG a single domain magnetic structure is created as we can see in Fig. 6, where we plot the intensities of some selected magnetic reflections as a function of the applied magnetic field. At the same time an induced ferromagnetic moment develops (increase of the intensity of the nuclear peaks), so the magnetic structure becomes conical. At high temperatures, in the regular helical structure range, this conical structure gradually evolves towards the saturated paramagnetic state as the field increases.

In the low-temperature region where third-order harmonics exist, however, we made the surprising observation that at higher fields the magnetic peaks that correspond to propagation vectors perpendicular to the field reappear and become dominant. Of course, the induced ferromagnetic component increases monotonically and at about 32 kG the

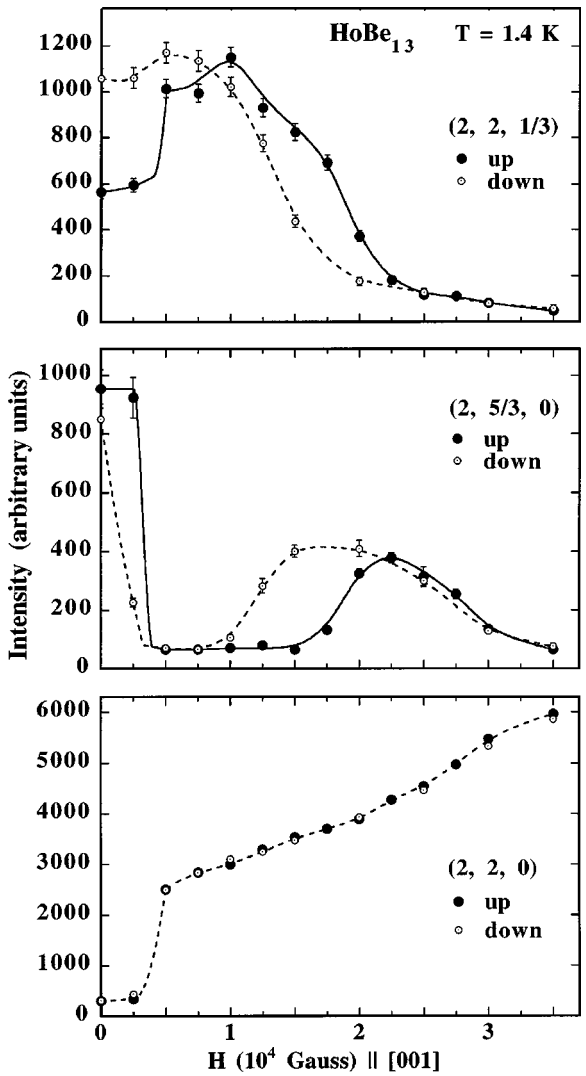

FIG. 6. Applied magnetic-field dependence of representative magnetic peaks at 1.4 K, with the field along the [001] direction. Shown are the $(2\ 2\ \frac{1}{3})$ and $(2\ \frac{5}{3}\ 0)$ reflections which propagate along and perpendicular to the field, respectively. We also show the (2 2 0) nuclear peak which increases as a result of the ferromagnetic contribution. Significant hysteresis effects are observed between the curves obtained with increasing or decreasing field.

antiferromagnetic structure is completely destroyed (Fig. 6) in good agreement with the magnetization measurements (Fig. 2). Integrated intensities of magnetic peaks were collected at 1.4 K in applied fields of 10, 15, 20, and 25 kG. To calculate the ferromagnetic component, the intensities of the nuclear Bragg reflections were also collected at the above field values. For the measurements of integrated intensities we always cooled the sample under magnetic field, starting from the paramagnetic state.

At 10 kG we have a single domain helical component propagating along the [001] direction and a induced ferromagnetic component, so the total arrangement is conical. The intensity ratios between first- and third-order harmonics is within statistical errors the same as at zero field, so the angle ϕ in our helical model does not change, and we get $m_h = 6.0(3)\mu_B$ for the magnetic moment of the helical component. From the nuclear intensities, which contain now a ferromagnetic contribution, we calculate a ferromagnetic

TABLE I. Observed integrated intensities of selected magnetic peaks of $HoBe_{13}$ at 1.4 K in various magnetic fields applied along the [001] direction. For each of the equivalent magnetic ordering wavevectors $[\frac{1}{3}\ 0\ 0]$, $[0\ \frac{1}{3}\ 0]$, and $[0\ 0\ \frac{1}{3}]$ the evolution of two first-order and one third-order reflection is presented. In all cases the sample was cooled under field starting from the paramagnetic state.

h	*k*	*l*	0 kG	10 kG	15 kG	20 kG	25 kG
$\frac{5}{3}$	0	0	2386(74)	29(7)	1002(32)	1035(33)	976(31)
$\frac{1}{3}$	2	0	1197(39)	0	39(8)	37(7)	34(7)
1	0	0	464(16)	0	188(8)	163(6)	98(6)
0	$\frac{5}{3}$	0	2057(64)	17(4)	960(31)	1034(33)	1057(34)
2	$\frac{1}{3}$	0	1090(39)	0	30(7)	27(7)	32(8)
0	1	0	418(15)	0	179(8)	173(6)	133(14)
2	2	$\frac{7}{3}$	1012(36)	1915(63)	840(29)	505(20)	129(10)
2	2	$\frac{1}{3}$	1160(39)	2075(67)	926(31)	557(21)	157(9)
2	2	1	212(12)	385(18)	170(9)	103(5)	24(7)

component of $m_f = 4.9(3)\mu_B$. Combining m_f (along c axis) and m_h (perpendicular to c) we get a total moment $m_t = 7.7(3)\mu_B$, in perfect agreement with our result at zero field.

The reason we preferred to describe the zero field structure with a helical rather than a transverse sinusoidal structure now becomes clear. If the structure at zero field was sinusoidal (squared at low temperatures), then for the reflections with propagation vectors perpendicular to the field we would expect a continuous decrease in intensity with increasing field. There would be no reason for their disappearance at intermediate field values and their reappearance at higher fields.

To understand the magnetic structure at higher fields we make the following observations from Table I, where we give the integrated intensities of some selected magnetic peaks at various field values. The intensities of the magnetic peaks with $\mathbf{k}=[0\ 0\ \frac{1}{3}]$ have always the same ratios between them, although they become smaller as the field increases. So this part is always due to the helical component we have already described. As the field increases, however, a progressively smaller volume fraction of the crystal is occupied by this structure. We also observe that while the $(\frac{5}{3}\ 0\ 0)$ peak reappears quite intense, the $(\frac{1}{3}\ 2\ 0)$ is now very weak. This means that the magnetic peaks with wave vectors along x and y are no longer due to a helical structure. Recalling that with neutrons we measure the component of the magnetic moment perpendicular to the scattering vector, it is easy to see that the magnetic structure responsible for the reappearance of those peaks is such that as we propagate along the x axis the moments are aligned in the y direction and vice versa.

We can consider two possibilities for this high-field magnetic structure. The first is to combine a single-**k** collinear component (with two domains) and the ferromagnetic component. This is a canted antiferromagnetic structure with total moments close to the [110] axes. The other choice involves a double-**k** noncollinear component with resulting moments close to the [111] axes. The two structures give equal neutron intensities and the same value for the total moment $7.7\mu_B$ which is in agreement with the magnetization measurements along the [110] axis. Therefore, on the following analysis we assume the single-**k** collinear component structure.

TABLE II. A summary of our results for the high magnetic-field magnetic structure of $HoBe_{13}$ at 1.4 K. The value of the ferromagnetic component, the ratio between the amplitudes of the first- and third-order harmonic of the canted structure, the fraction of the crystal volume ordered in this structure, the antiferromagnetic component of the moment, the angle between the total moment and the z axis, and the total magnetic moment are presented. The antiferromagnetic component is the same in both the canted and the conical structures, since this was our assumption in order to estimate the volume fractions.

H (kG)	m_{ferro} (μ_B)	m_1/m_3	V_{canted}	$m_{\text{antiferro}}$ (μ_B)	θ (m,z)	m_{total} (μ_B)
15	5.3(4)	4.3(4)	52(5)%	5.8(2)	48(3)°	7.8(4)
20	5.7(4)	4.9(4)	67(5)%	5.4(2)	44(3)°	7.8(4)
25	6.1(4)	5.7(6)	89(5)%	4.6(2)	37(3)°	7.6(4)

The simplest fixed moment collinear structure which would give rise to the observed magnetic peaks is a square wave arrangement. Three layers of ferromagnetically aligned Ho atoms are followed by three layers aligned in the opposite direction. In general, in the Fourier expansion of a square wave all the odd harmonics are included. In the particular case of $\mathbf{k}=[\frac{1}{3}\ 0\ 0]$, however, we can group the terms and we are left with a superposition of a sinusoidal wave with its third-order harmonic only,

$$m_y = \frac{4}{3} m \sin\left(2\pi \frac{1}{3} x\right) + \frac{1}{3} m \sin(2\pi x), \tag{9}$$

where the simplest choice for the phase has been made. For our calculation of magnetic intensities we use this decomposition with the coefficients replaced by m_1, m_3, the amplitudes of the first- and third-order harmonics, respectively. This is because in practice their ratio may not be exactly 4:1, due either to experimental accuracy or to the fact that the structure is not perfectly squared.

In the analysis, we assume that at each field value a fraction of the volume of the crystal orders in the conical structure propagating along the field as before. The rest orders in the new canted structure propagating in one of the two directions perpendicular to the field. By making the reasonable assumption that the total magnetic moment has to be the same throughout the volume of the crystal, we can estimate the volume fraction that is ordered in each of the states and put our results on an absolute scale. The agreement between calculated and observed intensities is always good and our results are summarized in Table II. The values obtained for the total magnetic moment are in good agreement with the magnetization measurements and our calculation for the zero-field magnetic structure. The ratio between first- and third-order amplitudes is very close to four at 15 kG but it becomes somewhat larger at higher fields. Contamination of the third-order harmonics by ferromagnetic contribution

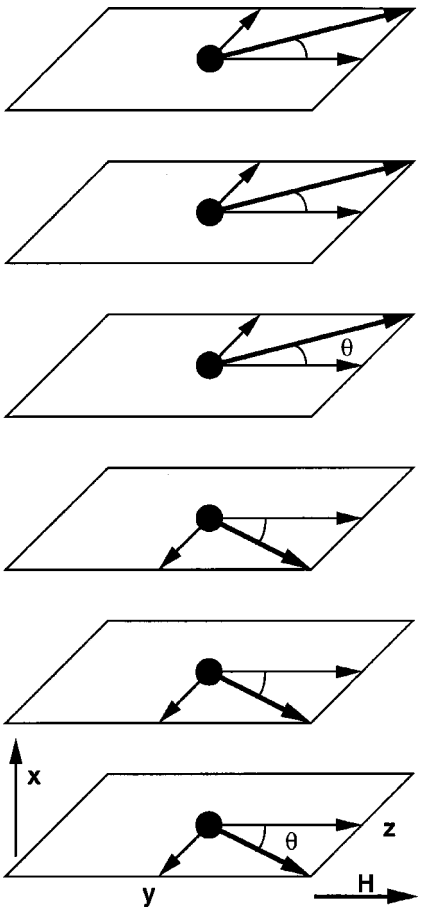

FIG. 7. The high-field canted magnetic structure of $HoBe_{13}$. The field is applied along the *z* axis giving a ferromagnetic component. As we move along the *x* direction, the antiferromagnetic component forms a transverse square wave $(+\ +\ +\ -\ -\ -)$ structure.

through the $\lambda/2$ would give the opposite effect. So we can say that the square wave magnetic structure becomes somewhat distorted as the system approaches the saturated paramagnetic state. In Fig. 7 we illustrate the high field canted magnetic structure of $HoBe_{13}$. In Fig. 8 we plot the field dependence of the volume fraction that orders in the canted magnetic structure, and the ratio of the antiferromagnetic component of the moment to the total moment.

We have also performed measurements with a magnetic field applied along the $[1\bar{1}0]$ direction. As shown in Fig. 9, and in agreement with the magnetization measurements, only one transition is observed. From 4 to 5 kG a strong ferromagnetic contribution develops abruptly and further increases more slowly with increasing field. The behavior of the antiferromagnetic intensities depends on the relative orientation of the field with respect to the propagation vector. The helical domain with $\mathbf{k}_z=[0\ \ 0\ \ \frac{1}{3}]$, which has no field component perpendicular to the moments, vanishes abruptly between 4 and 5 kG. The intensities of the other two domains, which are favored by a field component perpendicular to the moments, fall sharply at the transition to a lower value and then decrease continuously.

At 27 kG the ferromagnetic component along the field direction $[1\bar{1}0]$ is $7.1(2)\mu_B$ and the antiferromagnetic one is

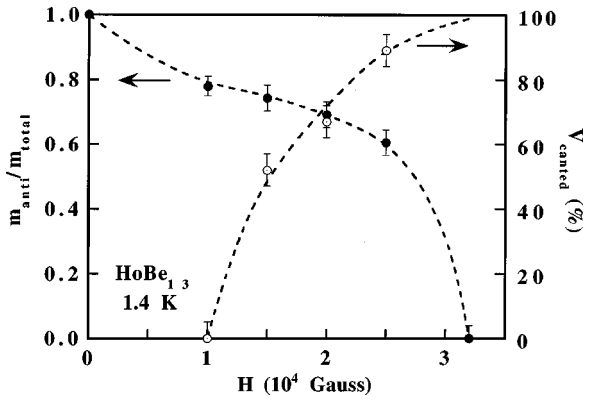

FIG. 8. Magnetic-field dependence of the volume fraction that orders in the canted magnetic structure and the ratio of the antiferromagnetic component (helical or collinear) to the total moment of $HoBe_{13}$ at 1.4 K.

$2.9(2)\mu_B$. Thus the total moment is $7.7(3)\mu_B$ per Ho ion, a value in agreement with a moment orientation along a [110] direction.

IV. CONCLUSION

A detailed study of the magnetic structure of $HoBe_{13}$ and its dependence on a magnetic field applied along the [001] and [110] directions has been carried out using neutron-diffraction techniques. For a field *H* applied along a cubic axis two metamagnetic transitions from a zero-field helical to a conical and then a canted structure have been evidenced. All these structures have the same magnetic ordering wave vector which is determined by the generalized susceptibility $\chi(q)$ of the conduction electrons, and the same resulting moments of $7.7(3)\mu_B$ along the [110] axes due to single ion anisotropy and the presence of exchange.

The magnetic phase diagram of $HoBe_{13}$ for a field along the [001] axis is presented in Fig. 10. The phase boundaries are drawn here for increasing magnetic field. It is evident,

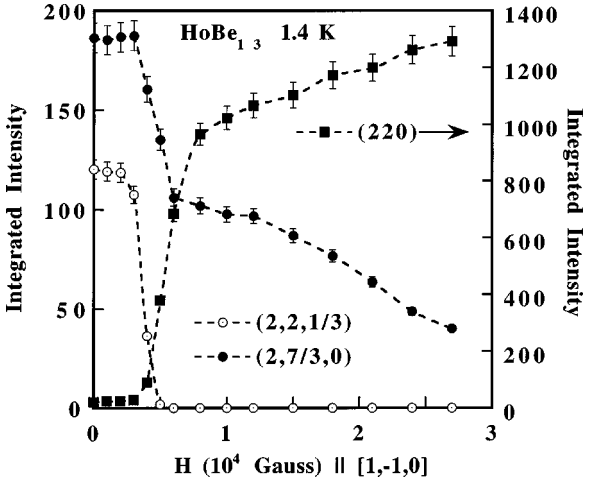

FIG. 9. Applied magnetic-field dependence of representative magnetic peaks at 1.4 K, with the field along the $[1\bar{1}0]$ direction. Shown are the $(2\ \ 2\ \ \frac{1}{3})$ and $(2\ \ \frac{7}{3}\ \ 0)$ reflections which propagate perpendicular and at 45° to the field, respectively, and the (2 2 0) nuclear peak which includes a ferromagnetic contribution.

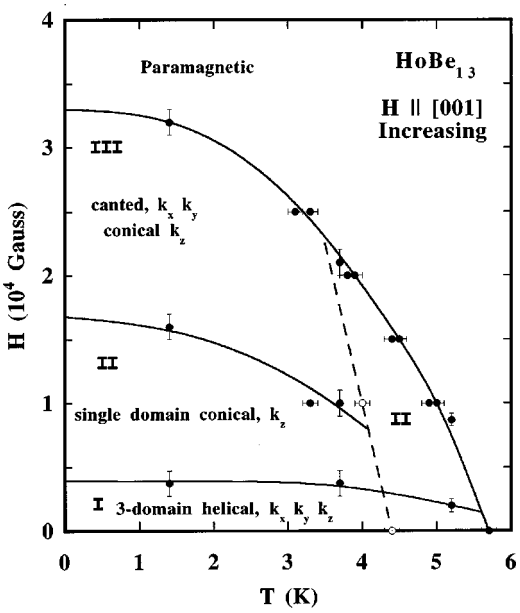

FIG. 10. Magnetic phase diagram of $HoBe_{13}$ at 1.4 K. The points mark the appearance (or disappearance) of magnetic reflections, and they were taken with increasing magnetic field or decreasing temperature. The full and open circles correspond to first and third order reflections respectively. Third-order harmonics exist to the left of the dashed line. Hysteresis effects will move the boundaries if the changes are made in the opposite sense, especially the boundary between phase *II* and *III*. In phase *III* the collinear structure coexists with the helical one. However, as the field increases the collinear structure becomes more and more dominant.

from the hysteresis effects observed in Fig. 6, that the boundaries would be displaced if the field decreases. The dashed line in the phase diagram marks the squaring up of the structure and the appearance of third-order harmonics. According to the previous powder study[6] it should also mark the commensurate-to-incommensurate transition. As we discussed earlier, however, our resolution was not good enough to establish the small change of the magnetic ordering wave vector. It would be of interest to perform a similar study on $TbBe_{13}$ if single crystals become available. In this compound ($T_N = 16.5$ K) the departure of the wave vector from the commensurate value is much greater ([0 0 0.312] at T_N)[3] and it should be easy to establish unambiguously.

For H along the [110] axis the phase diagram is simpler since only one metamagnetic transition leads from the helical magnetic structure to the saturated paramagnetic state. We have not undertaken a neutron experiment with H along the [111] direction, since it is obvious from the magnetization measurements that the helical state transforms in this case directly to the saturated paramagnetic one with moments along the field direction, which are now nearly equal to the maximum value allowed for Ho ions.

At low fields the behavior of $HoBe_{13}$ is dominated by the exchange interactions which lock the propagation vector $\mathbf{k} = [\frac{1}{3}\ 0\ 0]$. The crystal symmetry then implies a moment direction either perpendicular or parallel to **k**, while the single-ion anisotropy (CEF) would prefer a [111] moment orientation incompatible with the propagation vector. This provides a natural explanation for the appearance of the canted magnetic structure at high fields along the [001] axis. The canted structure has a total magnetic moment very close to a [101] axis which the system prefers in order to satisfy exchange and CEF effects.

ACKNOWLEDGMENTS

P.D. thanks the European Commission for financial support. Ames Laboratory is operated for the U.S. Department of Energy by Iowa State University under Contract No. W-7405-Eng-82. This work was supported by the Director for Energy Research, Office of Basic Sciences. Work at Florida was supported by the United States DOE under Contract No. DE-FG05-86ER45286.

*Also at the University of Augsburg, Memmingerstr. 6, 86159 Augsburg, Germany.

[1] E. Bucher, J.P. Maita, G.W. Hull, R.C. Fulton, and A.S. Cooper, Phys. Rev. B **11**, 440 (1975).

[2] A. Herr, M. J. Bensus, and A. Meyer (unpublished).

[3] F. Vigneron, M. Sougi, P. Meriel, A. Herr, and A. Meyer, J. Phys. (Paris) **41**, 123 (1980).

[4] F. Vigneron, M. Bonnet, A. Herr, and J. Schweizer, J. Phys. F **12**, 223 (1982).

[5] F. Vigneron, M. Bonnet, and J. Chappert, J. Phys. F **15**, 181 (1985).

[6] F. Vigneron, M. Bonnet, and P. Becker, Physica B **130**, 366 (1985).

[7] P.J. Becker, M. Bonnet, and F. Vigneron, Mol. Cryst. Liq. Cryst. **125**, 405 (1985).

[8] A. Hiess, M. Bonnet, P. Burlet, E. Ressouche, J.-P. Sanchez, J.C. Waerenborgh, S. Zwirner, F. Wastin, J. Rebizant, G.H. Lander, and J.L. Smith, Phys. Rev. Lett. **77**, 3917 (1996).

[9] R.H. Heffner, J.L. Smith, J.O. Willis, P. Birrer, C. Baines, F.N. Gyrax, B. Hitti, H.R. Ott, A. Schenck, E.A. Knetsch, J.A. Mydosh, and D.E. MacLaughlin, Phys. Rev. Lett. **65**, 2816 (1990); R.H. Heffner, J. Alloys Compd. **213-4**, 232 (1994).

[10] A.I. Goldman, S.M. Shapiro, G. Shirane, J.L. Smith, and Z. Fisk, Phys. Rev. B **33**, 1627 (1986).

[11] G.H. Lander, S.M. Shapiro, C. Vettier, and A.J. Dianoux, Phys. Rev. B **46**, 5387 (1992).

[12] P. Morin, J. Rouchy, and D. Schmitt, Phys. Rev. B **37**, 5401 (1988).

[13] M. T. Huchings, in *Solid State Physics: Advances in Research and Applications*, edited by F. Seitz and D. Turnball (Academic, New York, 1964), Vol. 16, p. 227.

[14] M. Bonnet (private communication).

[15] F. Vigneron, M. Bonnet, and R. Kahn, in *Crystalline Electric Field and Structural Effects in f-Electron Systems*, edited by J. E. Crow, R. P. Guertin, and T. W. Mihalisin (Plenum, New York, 1980).

[16] J. Rossat-Mignod, in *Magnetic Structures*, Methods of Experimental Physics Vol. 23C, edited by D. L. Price and K. Skold (Academic, New York, 1986).